JOURNAL OF AIRCRAFT
Vol. 46, No. 3, May–June 2009

Engineering Notes

ENGINEERING NOTES are short manuscripts describing new developments or important results of a preliminary nature. These Notes should not exceed 2500 words (where a figure or table counts as 200 words). Following informal review by the Editors, they may be published within a few months of the date of receipt. Style requirements are the same as for regular contributions (see inside back cover).

Unsteady Airfoil with Dynamic Leading- and Trailing-Edge Flaps

T. Lee* and P. Gerontakos†
McGill University, Montreal, Quebec H3A 2K6, Canada

DOI: 10.2514/1.42431

I. Introduction

THE dynamic overshoot in lift force and the accompanying large nose-down pitching moment observed on oscillating and pitching airfoils, as a result of the formation, convection, and shedding of an energetic dynamic-stall vortex (DSV), continue to make dynamic stall and its control an important topic in unsteady aerodynamics. Moreover, once the DSV passes the airfoil trailing edge and moves into the wake, the flow progresses to a state of poststall full separation over the upper surface and an abrupt loss of lift is incurred, causing a large degree of hysteresis in the lift coefficient. Various dynamic-stall flow control methods, such as trailing-edge flaps [1–5], pulsating and synthetic jets [6–8], leading-edge slots with and without blowing and suction [9,10], and dynamically deformable and variably drooped leading edges [11,12], etc., capable of minimizing, or eliminating, the hysteresis in the dynamic-C_l loop and the peak negative pitching-moment coefficient $C_{m,\text{peak}}$, have been proposed. It should, however, be noted that for rotorcraft, the dynamic-stall flow control is aimed at the prevention of the DSV occurrence and the mitigation of nose-down pitching moment on rotor blades, whereas for highly maneuverable aircraft, the purpose is to delay the DSV spillage and to enhance the dynamic lift. The trailing-edge flap (TEF) dynamic-flow control concept has been considered widely for dynamic lift enhancement and nose-down pitching-moment suppression. Trailing-edge flaps have also been used extensively as a routine practice of controlling the lift by temporarily altering airfoil camber on an airplane in steady-low-speed operations, especially during takeoff and landing, without penalizing cruise performance.

Rennie and Jumper [2] investigated the effectiveness of deflecting a 27% TEF control surface in negating the unsteady lift generated during a pitch motion of a NACA 0009 airfoil at $Re = 2 \times 10^5$. They reported that the dynamic TEF effectiveness was larger than the steady-state value and had direct ramifications on unsteady lift control. The effectiveness of a deflecting control surface was also found to be higher while the control surface was in motion and was rapidly decreased at large deflections, as a result of the thickening or separation of the boundary layer on the trailing-edge flap. Furthermore, the motion of TEF appeared to delay the occurrence of dynamic stall on the airfoil. Gerontakos and Lee [5] examined the alleviation of the nose-down pitching moment by using a 25%c TEF, actuated dynamically in response to the airfoil oscillation, at $Re = 1.65 \times 10^5$. The prescheduled TEF motion consisted of a brief pulse, represented by a constant ramp-up motion, remained steady briefly, and was followed by a constant ramp-down motion. They found that the reduction in $|-C_{m,\text{peak}}|$ was mainly a consequence of the suction pressure introduced on the lower surface of the upward deflected TEF and that a relatively early flap actuation (initiated between the static-stall angle α_{ss} and the maximum angle of attack $\alpha_{\max}$ during pitch-up) with a rather long duration (about half of the oscillation cycle time) and a maximum deflection $\delta_{\max} \geq 60\%\alpha_{\max}$ should be more effective at reducing the nose-down pitching-moment excursion, and, in the meantime, provide a good compromise between the various aerodynamic requirements. Also, the magnitude of the maximum lift coefficient $C_{l,\max}$ was found to be rather insensitive to the flap-actuation duration t_d, whereas the poststall lift was decreased with decreasing t_d. More important, the DSV formation and detachment were not affected by the upward TEF motion.

In addition, dynamic leading-edge-flap lift control has also been employed by researchers elsewhere to allow high-performance aircraft to achieve a rapid and sustained high-lift coefficient. The purpose of leading-edge devices is to increase camber and thus suppress leading-edge separation during rapid arbitrary airfoil pitching maneuvers. Rennie and Jumper [13] reported an experimental determination of a 20% leading-edge flap schedule used to maintain attached flow during arbitrary dynamic pitching motions of a NACA 0009 airfoil at $Re = 2 \times 10^5$. The leading-edge flap (LEF) schedule kept the flow attached dynamically at angles of attack that were separated during static tests. The use of the LEF avoided catastrophic dynamic-stall flow-separation events. Also, for a static leading-edge flap schedule, the attached flow could be maintained by keeping the leading-edge flap aligned with the oncoming flow. In summary, it is known that both leading- and trailing-edge flaps can serve to increase the camber and manage the boundary layer effectively and thus increase the maximum lift of an airfoil. However, despite much predictive work, published experimental data on the unsteady aerodynamic loads induced by the dynamically deflecting leading- and trailing-edge flaps are still sparse.

A preliminary experimental study was conducted to examine the effects of an 18%c leading- and a 25%c trailing-edge flap, actuated dynamically and independently, on the dynamic-load loops of a sinusoidally oscillating NACA 0015 airfoil in a subsonic wind tunnel at $Re = 2.86 \times 10^5$. The dynamic-load loops were obtained by integrating the unsteady surface pressure distributions. Both upward and downward flap deflections actuated at a fixed start time ($t_s = 0\pi$) were investigated. This t_s value was chosen to maximize the influence of the flap motion on the transient DSV-induced effects. Special emphasis was also placed on the simultaneous measurements of airfoil and flap deflection histories, synchronized with the surface pressure measurements.

II. Experimental Methods

The experiment was conducted in the $0.9 \times 1.2 \times 2.7$ m^3 suction-type wind tunnel at McGill University. A rectangular untwisted NACA 0015 airfoil, fabricated from solid aluminum, with a chord

Received 27 November 2008; revision received 20 February 2009; accepted for publication 20 February 2009.

*Associate Professor, Department of Mechanical Engineering. Member AIAA.

†Research Assistant; currently Aerospace Engineer, Bombardier Aerospace, Montreal, Quebec, Canada.

$c = 25.4$ cm and a span $b = 38$ cm, was used as the test model. The airfoil model was mounted horizontally at the center of the wind-tunnel test section and was equipped with end disks with a diameter of 50 cm to reduce the free-end effects. The gap between the airfoil model and the end plate was kept at less than 1 mm to minimize the leakage flow through the gap. The airfoil was oscillated beyond its static-stall angle of $\alpha_{ss} = 15$ deg with $\alpha(t) = 16\,\text{deg} + 8\,\text{deg}\sin\omega t$ (where $\omega = 2\pi f$, f is the oscillation frequency and t is the time) and κ ($\pi f c/u_\infty$, where u_∞ is the freestream velocity) of 0.1 by a specially designed four-bar linkage and flywheel oscillation mechanism. The oscillation frequency was monitored in real time by using a HP model 3581A spectral analyzer and was measured to an accuracy of ± 0.02 Hz. The airfoil pitch axis was located at the quarter-chord location. The effects of pitch axis on the lift-curve characteristics of a pitching airfoil were examined by Jumper et al. [14]. The instantaneous angle of attack $\alpha(t)$ of the airfoil and the phase reference signal were recorded from both the servomotor feedback resolver and a potentiometer mounted on the servomotor shaft. The chord Reynolds number was fixed at 2.86×10^5.

The wing was also equipped with a full-span $18\%c$ leading-edge flap (LEF) and a $25\%c$ TEF, which can be activated and deactivated independently and dynamically in response to the oscillating airfoil phase angle by a Maxon model RE-35 servomotor (Fig. 1a). The flap actuation employed a brief pulse and was actuated at any desired time and instantaneous angle of attack. The pulse signal was represented by a constant ramp-up motion, remained steady briefly, and was followed by a constant ramp-down motion through the use of a Maxon EPOS 70/10 programmable motion controller (Fig. 1b). In the present experiment, R_1 and R_2 were fixed at $11\%f^{-1}$, and t_d and $\delta_{\max}$ were fixed at $50\%f^{-1}$ and 15 deg ($62.5\%\alpha_{\max}$), respectively. The start time was fixed at $t_s = 0\pi$ (corresponding to a flap actuation initiated at $\alpha_u = \alpha_{\text{mean}} = 15$ deg), which was chosen to allow the actuation of the flap at around the onset of flow reversal during the second stage of the pitch-up motion. The selection of t_s, $\delta_{\max}$, t_d, R_1, and R_2 followed the suggestions of Gerontakos and Lee [5]. Note also that when the phase angle was within the range $-0.5\pi \le \tau \le 0.5\pi$, the airfoil was described to be in pitch-up; when $0.5\pi \le \tau \le 1.5\pi$, the airfoil was said to be in pitch-down.

The airfoil model was also equipped with 48 0.35-mm-diam pressure tabs, covering up to $x/c = 96.3\%$, distributed on the upper and lower airfoil surfaces. The surface pressure signals were recorded by using a fast-response Honeywell DRAL501 differential pressure transducer connected via a 48-port Scanivalve system and were phase-locked and ensemble-averaged over 95 cycles of oscillation to obtain the dynamic C_l–C_m–C_d loops. The transducer signals were low-pass-filtered and amplified with a multichannel AA Lab model G3006 pressure measurement system. The effects of the 39-cm-long and 0.75-mm-i.d. plastic tubing (separating the surface tap and the pressure transducer) on the unsteady pressure signals were examined by comparing the transducer output level and the phase with a controlled acoustic sound source. The effect of the length of the plastic tubing was found to be a simple time-constant delay on all pressure signals with frequency above 2.56 Hz, which rendered a limited reduced frequency κ of 0.116 at $u_\infty = 17.5$ m/s or $Re = 2.86 \times 10^5$ in the present experiment. An uncertainty analysis gives a typical total uncertainty ± 0.013 in the surface pressure coefficient C_p.

III. Results and Discussion

The effects of LEF motion (actuated at $t_s = 0\pi$ with $t_d = 50\%f^{-1}$, $R_1 = R_2 = 11\%f^{-1}$, and $\delta_{\max} = 15$ deg) on the dynamic-load loops

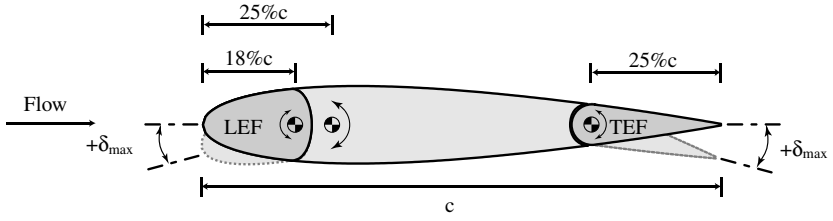

a)

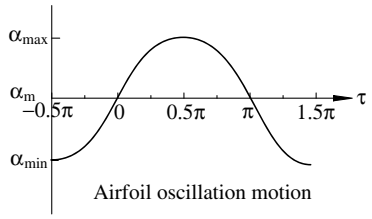

Airfoil oscillation motion

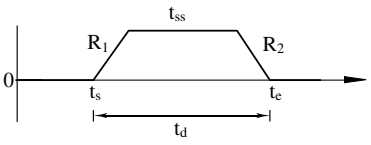

Flap motion profile

R_1	upward flap deflection ramp rate		
R_2	downward flap deflection ramp rate		
t_d	flap actuation duration	t_e	end of flap actuation
t_s	flap actuation start time	t_{ss}	steady-state time period

b)

Fig. 1 Schematics of a) airfoil model and b) flap-motion profile.

were examined first and are presented in Figs. 2a–2c. Also shown in Fig. 2 are the baseline, or uncontrolled, airfoil data, which show that the deep-stall airfoil oscillation led to a 62 and 227% increase in $C_{l,\max}$ and $|-C_{m,\text{peak}}|$, as well as a dynamic-stall angle $\alpha_{\text{ds}} = 22.8$ deg, compared with $\alpha_{\text{ss}} = 15$ deg of the static airfoil. The oscillating airfoil also produced a large hysteresis in the dynamic-C_l loop [or the C_l-hysteresis factor $C_H = \int C_l(\alpha)\mathrm{d}\alpha$], which is the source of reduced aerodynamic damping, which can potentially lead to a variety of aeroelastic problems on the rotor. The C_l-hysteresis can be attributed to the fact that full flow reattachment was not obtained until the airfoil was well below its normal α_{ss}, as a result of the lag induced by the reverse-kinematic-induced camber effect on the leading-edge pressure gradient by the negative pitch rate. The downward LEF control produced a 8% reduction in $C_{l,\max}$, compared with the baseline airfoil, whereas the dynamic-stall angle remained virtually unaffected (see the thin solid line in Fig. 2a). The surface pressure coefficient C_p data presented in Figs. 3a and 3b further indicate that this specific downward LEF deflection also led a more favorable pressure distribution with lower adverse pressure gradient near the leading edge and, more significantly, the disappearance of the DSV and its subsequent catastrophic spillage. The gain in the C_l created by the induced leading-edge camber effects and the relief of the severity of the adverse pressure gradient was dwarfed by the large loss in the dynamic overshoot (originated from the absence of the DSV). The avoidance of the DSV formation and its catastrophic spillage also produced a large recovery in C_l during poststall (see Fig. 3c), compared with the baseline airfoil; a 42% reduction in C_H was observed. The elimination of the DSV also led to a narrowed wake with a 10% reduction in the maximum drag coefficient $C_{d,\max}$, as well as a 23% improvement in peak negative C_m (see Fig. 2b). The values of $C_{l,\max}$, α_{ds}, $C_{m,\text{peak}}$, C_H, and $C_{d,\max}$ and the flap-motion profile are given in Table 1.

In contrast to the downward LEF motion, the DSV was promoted and detached sooner for upward LEF deflection (see Figs. 2a, 3a, and 3b); a $\alpha_{\text{ds}} = 21.6$ deg compared with 22.8 deg of the baseline airfoil was noticed. Note that for the baseline airfoil, the initiation of the

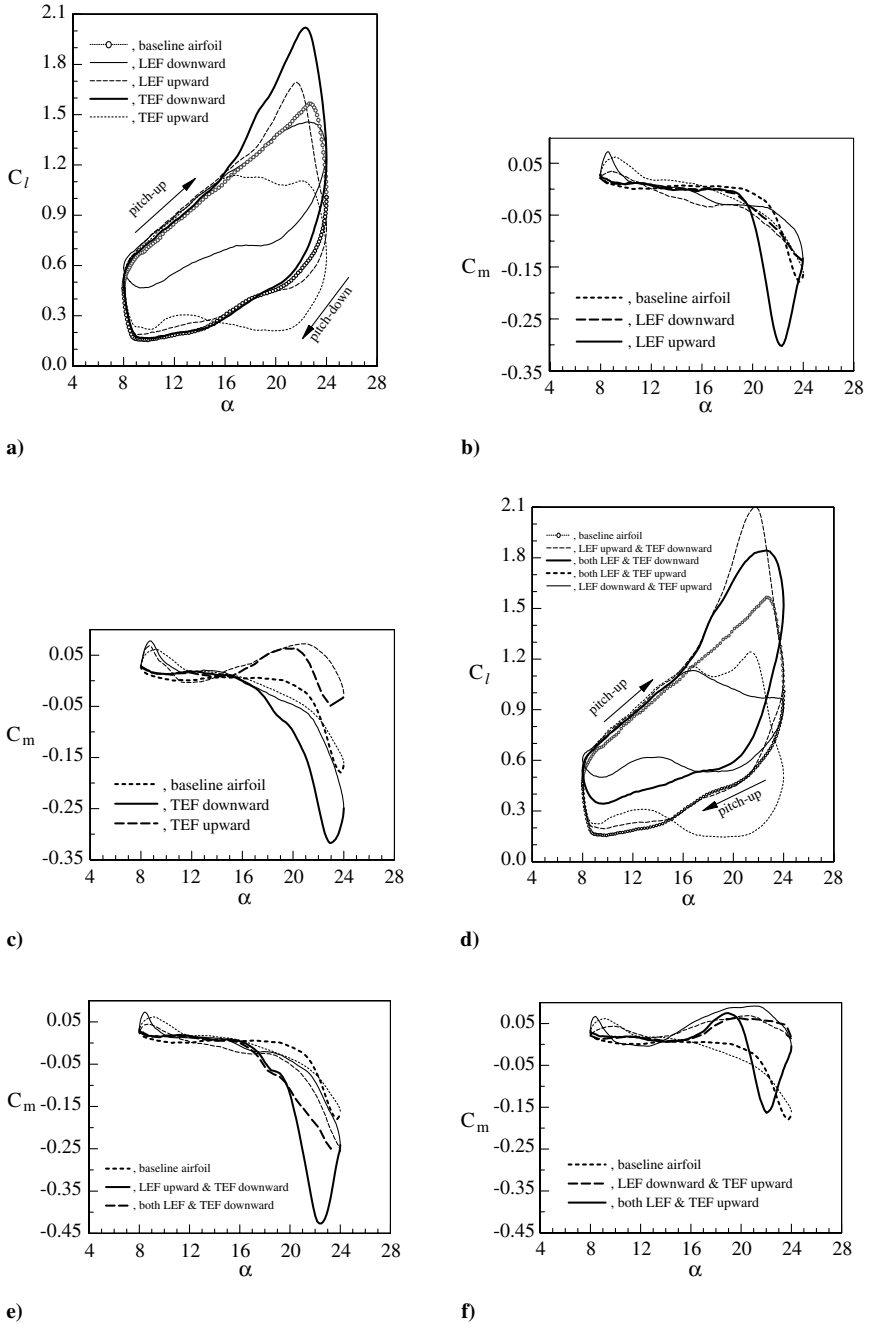

Fig. 2 Effects of a–c) individual and d–f) joint LEF and TEF control on dynamic-load loops.

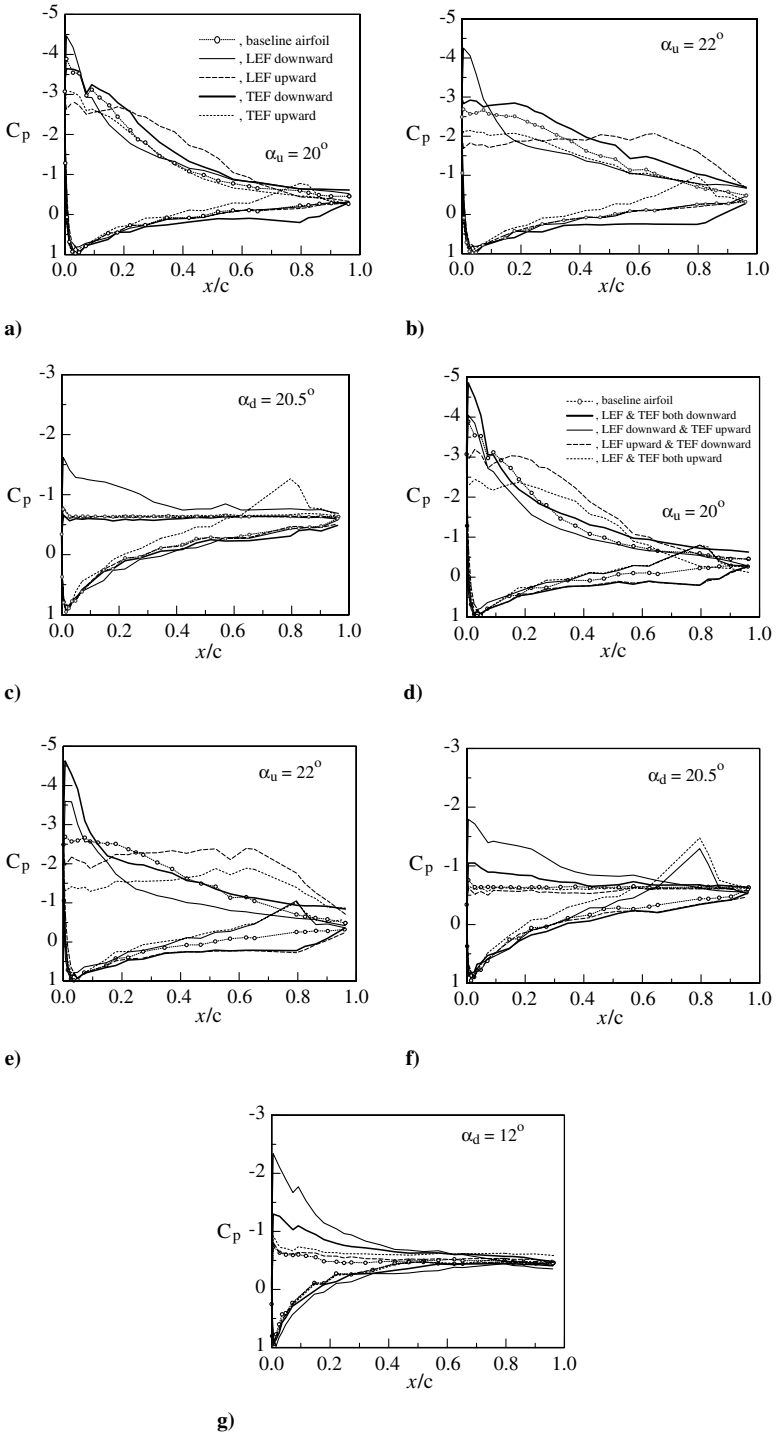

Fig. 3 Typical surface pressure coefficient distribution: a–c) individual LEF and TEF control and d–g) joint LEF and TEF control.

DSV (with an initial length of about $30\%c$) was originated from the disruption of the laminar separation bubble by the upstream movement of the flow reversal, or the so-called turbulent breakdown. The DSV then grew in size as it progressed downstream, and it detached abruptly from the airfoil upper surface as soon as it grew to the full length of the airfoil chord (at $\alpha_u \approx \alpha_{ds}$). The upward deflection of the LEF therefore triggered an earlier formation of the DSV (or, equivalently, a favorable DSV trapping) of an increased initial size and strength and thus an earlier DSV detachment or spillage. The strengthened DSV overwhelmed the loss in the leading-edge suction pressure, rendering a net 7% increase in $C_{l,\max}$. The poststall flow process, however, remained unchanged in comparison with the baseline airfoil (dashed line in Fig. 3c). The DSV promotion also resulted in a 67 and 13% increase in $|-C_{m,\text{peak}}|$ (see Fig. 2b) and $C_{d,\max}$, respectively. The effects of a shorter $t_d(=25\%f^{-1})$ on the critical airfoil aerodynamic characteristics were also examined (see cases C3–4 in Table 1); no significant discrepancy in the behavior of the dynamic-load loops, compared with the $t_d = 50\%f^{-1}$ control cases, was observed (see Table 1).

The TEF control, with downward or upward deflection, of the dynamic-load loops is presented in Figs. 2a and 2c. As expected, the downward TEF produced a considerable 27, 77, and 25% increase in $C_{l,\max}$, $|-C_{m,\text{peak}}|$, and $C_{d,\max}$, respectively, but only a slightly promoted α_{ds} (similar to the downward LEF control). The C_l enhancement was produced by flap-induced positive camber effects, especially in the trailing-edge region, and the increased pressures on both the lower and upper surfaces of the trailing-edge flap (solid line in Figs. 3a and 3b). Note that even though the downward TEF

Table 1 LEF and TEF motion profiles and airfoil performance

Case	LEF δ^b	LEF $t_d(f^{-1})$	LEF $t_s(\pi)$	TEF δ^b	TEF $t_d(f^{-1})$	TEF $t_s(\pi)$	$C_{l,\max}$	α_{ds}, deg	$C_{m,\text{peak}}$	C_H	$C_{d,\max}$
Static	——	——	——	——	——	——	0.98	15	−0.055	——	——
BA[a]	——	——	——	——	——	——	1.59	22.8	−0.180	11.86	0.60
C1	↓	0.5	0	——	——	——	1.46	22.9	−0.138	6.87	0.54
C2	↑	0.5	0	——	——	——	1.70	21.6	−0.302	12.47	0.68
C3	↑	0.25	0	——	——	——	1.69	21.2	−0.310	12.58	0.66
C4	↓	0.25	0	——	——	——	1.46	22.5	−0.150	10.20	0.55
C5	——	——	——	↓	0.5	0	2.02	22.4	−0.318	13.92	0.75
C6	——	——	——	↑	0.5	0	1.10	22.3	−0.057	11.35	0.46
C7	↑	0.5	0	↓	0.5	0	2.10	21.8	−0.429	14.50	0.81
C8	↓	0.5	0	↓	0.5	0	1.84	22.9	−0.260	10.45	0.53
C9	↓	0.5	0	↑	0.5	0	1.15	16.8	0.018	5.79	0.36
C10	↑	0.5	0	↑	0.5	0	1.25	21.5	−0.162	12.00	0.68

[a]BA denotes the baseline, or uncontrolled, oscillating airfoil.
[b]Symbols ↓ and ↑ denote flaps deflected downward and upward, respectively.

deflection generally caused a slightly promoted turbulent separation in the trailing-edge region, which, in turn, led to a somewhat earlier DSV spillage, the behavior of the DSV was, however, largely unaffected. Furthermore, no significant changes in the dynamic airload and flow process during poststall were observed, due to the fact that the flap was embedded in the DSV-induced separated flow. Note that the baseline, LEF-upward, TEF-upward and TEF-downward airfoils in Figs. 3a and 3b were all in various stages of dynamic stall so that their suction peaks were reduced and they exhibited a more-downstream pressure loading caused by the presence of a DSV over the top of the airfoil.

The undesired large increase in $|-C_{m,\text{peak}}|$ (characteristic of downward TEF deflection) can be alleviated by upward TEF motion; an 82% reduction in $|-C_{m,\text{peak}}|$ (see Fig. 2c), at the price of a 46% decrement in $C_{l,\max}$ (see Fig. 2a), mainly as a result of the substantial decrease in the pressure on the lower surface of the TEF (dotted line in Figs. 3a and 3b), was observed. It is of interest to note that the considerable decrease in the pressure on the flap lower surface not only rendered an unusual reduction in the dynamic lift force and stalling mechanism, but is also responsible for the large C_l decrement during poststall (Figs. 2a and 3c). The C_p data further demonstrate that the DSV was largely unaffected. In summary, it seems that the downward TEF motion had a dominant influence on the camber effects (i.e., more effective than changing the chord-line geometry at the leading-edge region) and was more effective at enhancing $C_{l,\max}$ than the LEF motion. The downward LEF deflection eliminated the DSV formation and was more effective at reducing the peak negative nose-down pitching moment. On the other hand, the upward LEF deflection promoted the DSV formation and detachment and always caused a large nose-down pitching-moment recovery. The upward TEF deflection made the ordinates of the mean camber line negative in the trailing-edge region and affected the pitching moment in a favorable manner. The joint LEF and TEF motion on the dynamic-load loops was therefore investigated.

Figures 2d–2f summarize the dynamic C_l and C_m loops for four different joint LEF and TEF motions actuated collectively at $t_s = 0\pi$ (see cases C7–C10 in Table 1). The largest increment in $C_{l,\max}$ was produced by the joint upward LEF and downward TEF deflection (denoted by the dashed line in Fig. 2d for case 7); a 32 and 22% increase in $C_{l,\max}$ and C_H compared with the baseline airfoil was obtained. This considerable $C_{l,\max}$ enhancement was, however, outperformed by the 1.38 times increase in $|-C_{m,\text{peak}}|$ (see Fig. 2e). The changes in $C_{l,\max}$, $|-C_{m,\text{peak}}|$, C_H, and $C_{d,\max}$ produced by a LEF, together with a downward TEF deflection (i.e., cases 7–8), can be obtained almost directly from the summation of the corresponding changes produced by the separate LEF and TEF motion (cases 1–6 in Table 1). It should, however, be noted that the most promising camber-adjusting techniques involving dynamically-deflected leading- and trailing-edge flaps should maximize the dynamic lift increment while keep the nose-down pitching moment as small as possible. For this purpose, the combined LEF and TEF control with collective downward deflection was examined (i.e., case C8). A $C_{l,\max}$ of 1.84 and $C_{m,\text{peak}}$ of −0.26, compared with 1.59 and −0.18 of the baseline airfoil, was obtained, which also translates into a 12% reduction in $C_{l,\max}$ and a 40% recovery in $|-C_{m,\text{peak}}|$ over the results created by the joint upward LEF and downward TEF control (i.e., case 7). The increase in $C_{l,\max}$ was due to the pressure increase on both the trailing-edge flap surfaces and the increase in the leading-edge suction pressure (see Figs. 3d and 3e). The reduction in $|-C_{m,\text{peak}}|$ was, however, attributed to the avoidance of the DSV formation. Note that the case 8 flap control also gave rise to an increased C_l and C_m during poststall (see Figs. 2d and 2e), as a result of the large increase in the surface pressures on the upper and lower surfaces downstream of the midchord of the airfoil (see Figs. 3e and 3f). The recovery in C_l during poststall (see Figs. 3f and 3g) also resulted in a 12% reduction in the dynamic C_l-hysteresis.

The TEF of the joint LEF/TEF control was also deflected upward to alleviate the detrimental nose-down pitching moment created by the control cases 7 and 8 (see Table 1). There was an upward shift of the C_m loop with a peak nose-up C_m value of +0.018, at the price of a 28% reduction in $C_{l,\max}$ (see Figs. 2d–2f), as a result of the DSV elimination and the large pressure decrement on the lower TEF surface (see Figs. 3d and 3e). The loss in C_l outweighed the gain in the suction pressure in the leading-edge region (produced by the joint downward LEF control). Particular attention should also be given to the unusual dynamic-stall mechanism and the drop in the dynamic C_l value between α_{mean} and $\alpha_{\max}$. The absence of the DSV and the increase leading-edge suction pressure also led to a considerably increased C_l during poststall in comparison with the baseline airfoil (see Figs. 3f and 3g). However, in contrast to the dominant downward TEF-induced positive camber effects, which permit the aerodynamic performance of the joint LEF/TEF control be inferred directly from the individual LEF and TEF control (e.g., cases 7 and 8), no simple relationship between the joint flap control with upward TEF deflection (i.e., cases 9 and 10) and the corresponding individual flap control was obtained. Finally, the LEF was also deflected upward (i.e., case 10) to compensate for the large $C_{l,\max}$ reduction incurred by the upward TEF deflection. Similar to the individual LEF control (i.e., case 2), the earlier presence of the DSV, of a weaker strength, was found to cause a 9% recovery in $C_{l,\max}$ but a peak negative C_m of −0.162. Meanwhile, the beneficial DSV-induced transient effects were, however, offset by the decreased pressure on the TEF lower surface (see Figs. 3d and 3e).

IV. Conclusions

A preliminary study of the control of the dynamic-load loops of an oscillating NACA 0015 airfoil via an 18%c LEF and a 25%c TEF, deflected dynamically and independently, was conducted at $Re = 2.86 \times 10^6$. Both upward and downward deflections actuated at $t_s = 0\pi$ (or α_{mean}) were tested to maximize the effects of the flap motion on the behavior of the DSV. The results show that deflecting the LEF alone did not have as large an effect on airfoil performance as deflecting the TEF. The downward LEF motion suppressed leading-

edge separation and eliminated the occurrence of the DSV, leading to a minor reduction in $C_{l,\max}$ but a considerably improved poststall lift condition, compared with the baseline airfoil. On the other hand, the upward LEF motion caused an earlier formation and shedding of the DSV and, subsequently, an increased $C_{l,\max}$ and negative peak C_m value. The downward TEF deflection always increased the lift. The formation and detachment of the DSV was, however, largely unaffected. The $C_{l,\max}$ enhancement was mainly due to pressure increases on both the lower and upper surfaces of the flap. The preliminary study further indicates that the joint upward LEF and downward TEF control produced the largest $C_{l,\max}$ and nose-down $C_{m,\text{peak}}$ among all the cases considered and that the net changes in the aerodynamic performance of the joint LEF/TEF with the TEF deflecting downward can be obtained from the accumulation of the performance produced by individual LEF and TEF control. Further investigations of LEF and TEF of different deflection amplitudes, actuation start times, and durations are, however, needed to support the findings reported.

Acknowledgments

This work was supported by the Natural Science and Engineering Research Council (NSERC) of Canada. L. S. Ko is thanked for undertaking the wind-tunnel tests.

References

[1] Vipperman, J. S., Clark, R. L., Conner, M., and Dowell, E. H., "Experimental Active Control of a Typical Section Using a Trailing-Edge Flap," *Journal of Aircraft*, Vol. 35, No. 2, 1998, pp. 224–229. doi:10.2514/2.2312

[2] Rennie, R., and Jumper, E. J., "Experimental Measurements of Dynamic Control Surface Effectiveness," *Journal of Aircraft*, Vol. 33, No. 5, 1996, pp. 880–887. doi:10.2514/3.47030

[3] Zhang, J., Smith, E. C., and Wang, K. W., "Active-Passive Hybrid Optimization of Rotor Blades with Trailing-Edge Flaps," *Journal of the American Helicopter Society*, Vol. 49, No. 1, 2004, pp. 54–65. doi:10.4050/JAHS.49.54

[4] Krzysiak, A., and Narkiewicz, J., "Aerodynamic Loads on Airfoil with Trailing-Edge Flap Pitching with Different Frequencies," *Journal of Aircraft*, Vol. 43, No. 2, 2006, pp. 407–418. doi:10.2514/1.15597

[5] Gerontakos, P., and Lee, T., "Dynamic-Stall Flow Control via a Trailing-Debs-Edge Flap," *AIAA Journal*, Vol. 44, No. 3, 2006, pp. 469–480. doi:10.2514/1.17263

[6] Smith, B. L., and Glezer, A., "The Formation and Evolution of Synthetic Jets," *Physics of Fluids*, Vol. 10, No. 9, 1998, pp. 2281–2297. doi:10.1063/1.869828

[7] Lorber, P. F., Carta, F. O., and Carlson, R. G., "The Aerodynamics of an Oscillating Jet Flap," *Journal of the American Helicopter Society*, Vol. 34, No. 2, 1989, pp. 24–32. doi:10.4050/JAHS.34.24

[8] Greenbaltt, D., and Wygnanski, I., "Dynamic Stall Control by Periodic Excitation, Part 1: NACA 0015 Parametric Study," *Journal of Aircraft*, Vol. 38, No. 3, 2001, pp. 430–438. doi:10.2514/2.2810

[9] Karim, M. A., and Acharya, M., "Suppression of Dynamic-Stall Vortices over Pitching Airfoils by Leading-Edge Suction," *AIAA Journal*, Vol. 32, No. 8, 1994, pp. 1647–1655. doi:10.2514/3.12155

[10] Ekaterinaris, J. A., "Numerical Investigations of Dynamic Stall Active Control for Incompressible and Compressible Flows," *Journal of Aircraft*, Vol. 39, No. 1, 2002, pp. 71–78. doi:10.2514/2.2897

[11] Chandrasekhara, M. S., Wilder, M. C., and Carr, L. W., "Unsteady Stall Control Using Dynamically Deforming Airfoils," *AIAA Journal*, Vol. 36, No. 10, 1998, pp. 1792–1800. doi:10.2514/2.294

[12] Chandrasekhara, M. S., Martin, P. B., and Tung, C., "Compressible Dynamic Stall Control Using a Variable Leading Edge Airfoil," *Journal of Aircraft*, Vol. 41, No. 4, 2004, pp. 862–869. doi:10.2514/1.472

[13] Rennie, R. M., and Jumper, E. J., "Dynamic Leading-Edge Flap Scheduling," *Journal of Aircraft*, Vol. 34, No. 5, 1997, pp. 606–611. doi:10.2514/2.2236

[14] Jumper, E. J., Schreck, S. J., and Dimmick, R. L., "Lift-Curve Characteristics for an Pitching Airfoil at Constant Rate," *Journal of Aircraft*, Vol. 24, No. 10, 1987, pp. 680–687. doi:10.2514/3.45507